Development of Large-Eddy Simulation Combustion Models for Thermodiffusive Instabilities in Turbulent Hydrogen Flames

By L. Berger†, A. Attili‡, J. Wang, K. Maeda AND H. Pitsch†

Lean premixed hydrogen flames are prone to thermodiffusive instabilities, which arise from the strong differential diffusion of hydrogen. These instabilities have a leading order effect on the flame dynamics and can enhance flame speeds by several times. Present combustion models cannot reproduce the effects of such instabilities and strongly mispredict the overall flame dynamics and flame speeds. In this work, a combustion model for large-eddy simulations (LES) that accounts for thermodiffusive instabilities is analyzed using detailed data from a direct numerical simulation (DNS) of a thermodiffusively unstable hydrogen/air flame. Based on the DNS data, progress variable and mixture fraction are rigorously identified as suitable model input parameters. The instantaneous flame state is modeled by a series of unstretched flamelets with varying equivalence ratios, while subfilter fluctuations are modeled with a presumed probability distribution. In an *a-priori* assessment, the newly proposed model shows a significant reduction of modeling errors in comparison to models that do not account for thermodiffusive instabilities.

1. Introduction

The recent rise of renewable energy sources is promoting the use of hydrogen as a carbon-free energy carrier (Perner & Bothe 2018). One possibility to harness the energy stored in hydrogen is its usage in thermochemical energy conversion processes such as in gas turbines, industrial burners, or piston engines (Sartbaeva *et al.* 2008). However, lean hydrogen/air flames are prone to intrinsic combustion instabilities and, in particular, thermodiffusive instabilities, which can substantially change flame dynamics, heat release rates and flame speeds. Thermodiffusive instabilities originate from the low Lewis number of hydrogen, which represents the ratio of the thermal and mass diffusivity, where the latter is particularly high for hydrogen. The strong differential diffusion of hydrogen leads to an amplification of small flame front perturbations such that strongly wrinkled flame fronts are observed with a significantly enhanced flame speed and strong variations of the local reaction rates (Matalon 2007). In a recent work, Berger *et al.* (2019) showed that thermodiffusive instabilities can lead to a fourfold increase flame speeds compared to the unstretched laminar burning velocity in laminar lean hydrogen/air mixtures at ambient conditions. In turbulent flames, Aspden *et al.* (2011) showed that the effects of thermodiffusive instabilities are present for a large range of Karlovitz numbers relevant for industrial applications. Most remarkably, thermodiffusive instabilities exhibit synergistic interactions with turbulent flows, leading to a further amplification of the turbulent flame

† Institute for Combustion Technology, RWTH Aachen University, Germany
‡ Institute for Multiscale Thermofluids, School of Engineering, University of Edinburgh, United Kingdom
† Institute for Combustion Technology, RWTH Aachen University, Germany

speed (Berger *et al.* 2022*b*). This results from high curvature and strain rate values in the turbulent environment, which further enhance the effects of differential diffusion. This leads to a strong enhancement of the local reactivity and local flame speed, which was similarly observed by Ahmed *et al.* (2021), who experimentally investigated turbulent spherically expanding hydrogen flames.

1.1. *Modeling framework*

As thermodiffusive instabilities have a leading order effect on the flame dynamics of laminar and turbulent hydrogen flames, accurate models considering these effects are of utmost importance to enable predictive simulations of hydrogen flames. To capture the effects of such instabilities in premixed hydrogen/air flames, a model needs to account for the differential diffusion of the fuel with respect to all other scalars, such as temperature, oxidizer and the combustion product. Bastiaans *et al.* (2007) proposed to solve transport equations for a hydrogen-based progress variable and temperature. A similar idea was pursued by Regele *et al.* (2013) and Schlup & Blanquart (2019). They suggest solving transport equations for a water-based progress variable and a mixture fraction based on the species mass fractions, which represents a local equivalence ratio and, hence, explicitly represents the effects of differential diffusion. One particular advantage of this formulation is that only the source term of progress variable requires modeling, as the transport equation of mixture fraction is already closed. Thus, the modeling approach of Regele *et al.* (2013) and Schlup & Blanquart (2019) is chosen as a baseline in this work, while modifications are proposed to adapt the model to turbulent flows.

In these approaches, the progress variable source term $\dot{\omega}_\mathrm{C}$ needs be modeled as a function of two transported scalars. Regele *et al.* (2013) and Bastiaans *et al.* (2007) proposed to represent the local flame state, which is parameterized by the two transported scalars, by a set of unstretched premixed flamelets with different equivalence ratios. Essentially, the variation of the global equivalence ratio of the flamelets mimics the local variations of the equivalence ratio due to differential diffusion effects within the flame front. In this way, a large portion of the flame state can be covered and good *a-priori* and *a-posteriori* predictions are achieved in laminar hydrogen flames. For this, planar hydrogen flames that develop corrugations due to the instabilities and one-dimensional canonical configurations, such as spherical flames, have been studied (Regele *et al.* 2013).

1.2. *Objectives and outline*

The aforementioned models are found to perform well for laminar flames, but due to the lack of high-fidelity data, their performance has yet not been assessed in turbulent flames. In turbulent flames, it is unclear whether a source term model can be built based on unstretched premixed flamelets similar to the laminar flames, as remarkably high values of curvature and strain rate are frequent in the turbulent environment. Whether these more extreme flame states can be well represented by unstretched premixed flamelets needs to be analyzed. Further, to utilize the models in large-eddy simulations (LES), models for the turbulence/flame subfilter interactions still need to be developed.

The objective of this work is to develop an LES combustion model for turbulent hydrogen flames — in particular, for the progress variable source term — that accounts for the effects of thermodiffusive instabilities. For model development and validation, the direct numerical simulation (DNS) data of Berger *et al.* (2022*b*) are employed in an *a-priori* analysis.

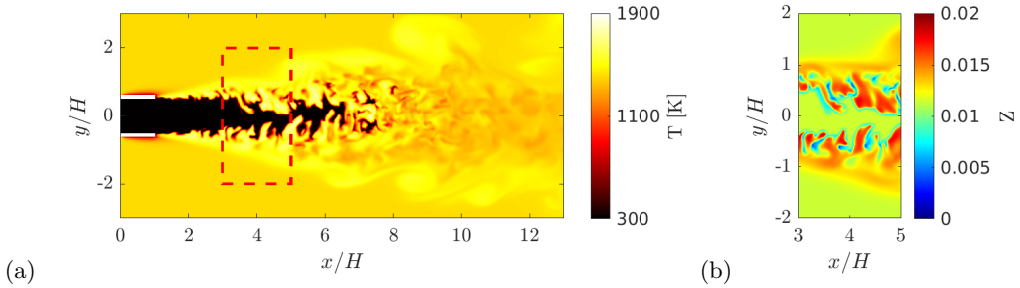

FIGURE 1. (a) Instantaneous temperature field of the DNS of a hydrogen/air flame in a slot burner configuration and (b) mixture fraction field for the dashed red box in panel (a).

2. DNS data set for a-priori analysis

For the *a-priori* analysis, the large-scale DNS of a lean hydrogen/air flame in a slot burner configuration of Berger *et al.* (2022*b*) is employed. The DNS was performed at a jet Reynolds number of $Re = 11,000$ and a Karlovitz number of $Ka \approx 15$ using detailed chemistry. A snapshot of the temperature field is shown in Figure 1(a). Unburned mixture is injected within the slot and burned gas is used as a coflow. The unburned mixture features an equivalence ratio of $\phi = 0.4$, a temperature of $T_\mathrm{u} = 298$ K and a pressure of 1 bar. The coflow gas is at the adiabatic flame temperature and from Figure 1(a) it is evident that super-adiabatic temperatures prevail in the hydrogen/air flame. This is a clear marker of thermodiffusive instabilities and has been discussed in detail by Giannakopoulos *et al.* (2015). In particular, the differential diffusion of hydrogen within the flame front leads to locally leaner and richer mixtures and, as discussed by Berger *et al.* (2022*b*), locally richer mixtures are preferentially formed due to the positive mean strain rate in the turbulent flow (Luca *et al.* 2019). In Figure 1(b), the fluctuations of the local equivalence ratio are shown by means of mixture fraction, which is introduced in the following.

3. Model development and analysis

3.1. *Definition of progress variable and mixture fraction*

A progress variable based on the hydrogen mass fraction is defined as

$$C = 1 - Y_{\mathrm{H_2}}/Y_{\mathrm{H_2,u}}, \tag{3.1}$$

where $Y_{\mathrm{H_2,u}}$ is the value of the hydrogen mass fraction $Y_{\mathrm{H_2}}$ in the unburned gas. While a progress variable could be also defined based on the mass fraction of water, Berger *et al.* (2022*a*) showed that such a progress variable possesses sub- and super-equilibrium values in the post flame region similar to the temperature, so unity values that typically define the burned gas are ambiguous. In contrast, the fuel is always fully consumed, so the value $C = 1$ unambiguously defines the burned gas. Further, the property that C is strictly bound to $C \in [0, 1]$ is important for the formulation of a model for the subfilter probability density function (PDF), as discussed further below. Therefore, a hydrogen-based progress variable C is used in the following analysis.

The effects of differential diffusion, e.g., the super-adiabatic temperatures in Figure 1(a), result from variations of the local equivalence ratio. The latter can be expressed by means of the mixture fraction Z, which is defined according to Bilger *et al.* (1990) as

$$Z = \frac{Z_\mathrm{H} + \nu(Y_{\mathrm{O_2,air}} - Z_\mathrm{O})}{1 + \nu Y_{\mathrm{O_2,air}}}. \tag{3.2}$$

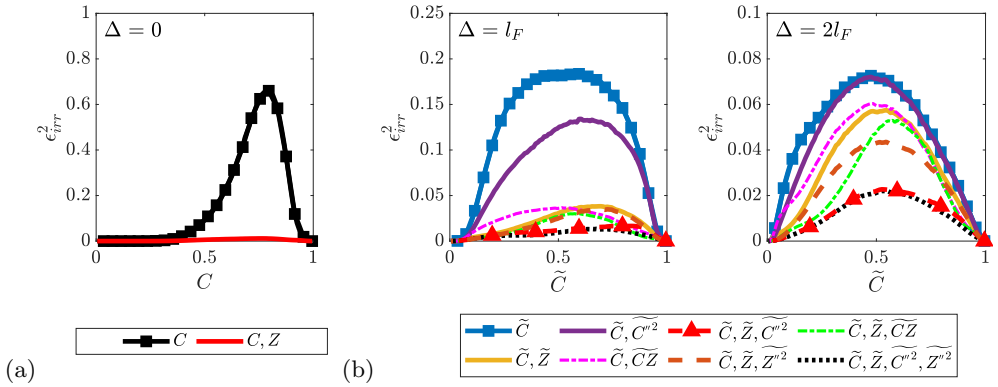

FIGURE 2. Irreducible errors of progress variable source term using different sets of parameters: analysis for (a) unfiltered fields and (b) filtered fields with two different filter sizes Δ.

The stoichiometric coefficient ν is defined by the ratio of the molar masses of oxygen and hydrogen as $\nu = 2M_{\mathrm{H}_2}/M_{\mathrm{O}_2}$, Z_{H} and Z_{O} represent the element mass fractions of hydrogen and oxygen, respectively, and $Y_{\mathrm{O}_2,\mathrm{air}}$ is the mass fraction of oxygen in air. As shown in Figure 1(b), strong fluctuations of the mixture fraction prevail in the turbulent flame due to the effects of differential diffusion.

3.2. *Optimal estimator analysis*

For the systematic development of any model, it is important to first identify the relevant input parameters, with which the quantity of interest can be best parameterized. This is achieved in an optimal estimator analysis, in which the capability of a set of parameters $\boldsymbol{\psi}$, e.g., $\boldsymbol{\psi} = [C, Z]$, to parameterize a target quantity Q, e.g., $Q = \dot{\omega}_{\mathrm{C}}$, is quantified by an error norm referred to as irreducible error. The amount of scatter of Q with respect to the conditional mean $\langle Q|\boldsymbol{\psi}\rangle$ is measured by the quadratic error norm and the parameterization is good if small irreducible errors are observed. In the following, the irreducible errors are conditionally averaged with respect to progress variable, yielding

$$\epsilon^2_{\mathrm{irr}^*} = \langle \left(\dot{\omega}_{\mathrm{C}} - \langle \dot{\omega}_{\mathrm{C}}|\boldsymbol{\psi}\rangle\right)^2 \mid C \rangle. \tag{3.3}$$

The irreducible error $\epsilon^2_{\mathrm{irr}^*}$ is normalized by the maximum value of the conditionally averaged source term $\langle \dot{\omega}_{\mathrm{C}}|C\rangle$, yielding

$$\epsilon^2_{\mathrm{irr}} = \frac{\epsilon^2_{\mathrm{irr}^*}}{\max(\langle \dot{\omega}_{\mathrm{C}}|C\rangle)^2}. \tag{3.4}$$

With this normalization, a value of unity indicates irreducible errors that are as large as the maximum value of the average source term within the flame front.

Figure 2 shows the irreducible errors for different parameterizations of the progress variable source term with different sets of parameters. As the development of an LES combustion model is pursued, three different filter sizes are shown: the unfiltered fields and two filter sizes Δ that correspond to one and two flame thicknesses l_{F}. l_{F} is the thermal flame thickness based on the temperature gradient of an unstretched flamelet at the conditions of the unburned gas. For the filtering procedure, a box filter of size Δ is used.

For the unfiltered fields, irreducible errors are shown if the progress variable source term is parameterized only by progress variable, e.g., $\boldsymbol{\psi} = [C]$, or by progress variable and mixture fraction, e.g., $\boldsymbol{\psi} = [C, Z]$. Consistent with the analyses of Berger *et al.* (2022*a*), including mixture fraction significantly improves the parameterization of the

source term, as it intrinsically captures the effects of differential diffusion. Thus, the instantaneous progress variable source term $\dot{\omega}_C$ may be expressed as $\dot{\omega}_C(C, Z)$.

For the filtered fields, additional input parameters need to be considered to parameterize the filtered progress variable source term $\overline{\dot{\omega}}_C$. Note that the overline denotes a Reynolds average and the tilde represents the density-weighted Favre averaging. The progress variable source term is Reynolds averaged, while progress variable $\widetilde{C}$ and mixture fraction $\widetilde{Z}$ are Favre averaged since in LES, a transport equation for $(\overline{\rho}\widetilde{C})$ is solved, which includes a Reynolds-averaged source term (Knudsen *et al.* 2013). While the instantaneous progress variable source term $\dot{\omega}_C$ only depends on progress variable and mixture fraction, the filtered progress variable source term $\overline{\dot{\omega}}_C$ is also affected by the subfilter distribution, which can be represented by the higher-order moments of progress variable and mixture fraction, such as $\widetilde{C}$, $\widetilde{Z}$, $\widetilde{C''^2}$ etc. This can be formally written as

$$\overline{\dot{\omega}}_C = \overline{\dot{\omega}}_C(\widetilde{C}, \widetilde{Z}, \widetilde{C''^2}, \widetilde{Z''^2}, \widetilde{CZ}, ...). \tag{3.5}$$

Thus, for the filtered fields, irreducible errors of several more different parameter sets are investigated in Figure 2(b) as combinations of different subfilter moments are assessed.

While progress variable and mixture fraction describe the unfiltered source term very well, their parameterization capability is significantly reduced for increasing filter sizes. In particular, the irreducible error of $\boldsymbol{\psi} = [\widetilde{C}, \widetilde{Z}]$ is close to $\boldsymbol{\psi} = [\widetilde{C}]$ in the right panel of Figure 2(b). Also, using only progress variable and one higher moment, e.g, $\widetilde{C''^2}$, $\widetilde{Z''^2}$ or $\widetilde{CZ}$, does not reduce irreducible errors significantly. Instead, three parameters are needed and the best parameterization is achieved with the set $\boldsymbol{\psi} = [\widetilde{C}, \widetilde{Z}, \widetilde{C''^2}]$. However, adding a fourth parameter, e.g., a second variance, does not yield any significant further reduction and, hence, is not needed. Thus, an LES combustion model for thermodiffusively unstable flames should be based on progress variable, mixture fraction and the variance of progress variable, where the latter accounts for the effect of filtering.

3.3. *Model formulation*

Based on the findings of the optimal estimator analysis, a model for the progress variable source term is formulated in this section. For this, a presumed PDF approach is chosen and the filtered progress variable source term $\overline{\dot{\omega}}_C$ is expressed as

$$\overline{\dot{\omega}}_C = \int \mathcal{P}(C, Z) \cdot \dot{\omega}_C(C, Z) \, \mathrm{d}C\mathrm{d}Z. \tag{3.6}$$

$\mathcal{P}(C, Z)$ is the joint subfilter distribution of progress variable and mixture fraction.

In a first step, a model for $\dot{\omega}_C(C, Z)$ is required. For this, Figure 3 shows the joint distribution of progress variable and mixture fraction, which indicates the range of possible states in the turbulent flame, and compares different sets of representative flamelets with the turbulent flame state. In Figure 3(a), strained flamelets with different strain rate a and an equivalence ratio of $\phi = 0.4$ are shown. These flamelets can be generated in FlameMaster (Pitsch 1998) by computing a counterflow flame, in which burned and unburned mixture are injected toward each other. Both streams feature an equivalence ratio of $\phi = 0.4$ and a pressure of $p = 1$ bar, while the temperatures are set to $T_\mathrm{u} = 298$ K in the unburned gas and to $T_\mathrm{b} = 1418$ K in the burned gas, where the latter represents the adiabatic flame temperature. The outermost flamelets represent the unstretched flamelet (dotted black curve) and the conditions when extinction occurs (yellow curve). In Figure 3(b), the joint distribution is compared to a set of unstretched premixed flamelets

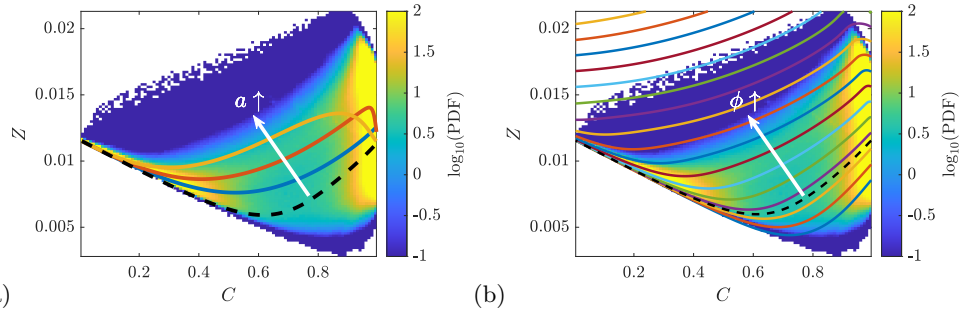

FIGURE 3. Joint distribution of progress variable and mixture fraction in the turbulent flame (a) overlaid by strained flamelets with different strain rate a obtained from a premixed counterflow flame, where the outermost flamelets represent the unstretched flamelet and the flamelet prior to extinction, and (b) overlaid by unstretched flamelets with different equivalence ratios ϕ.

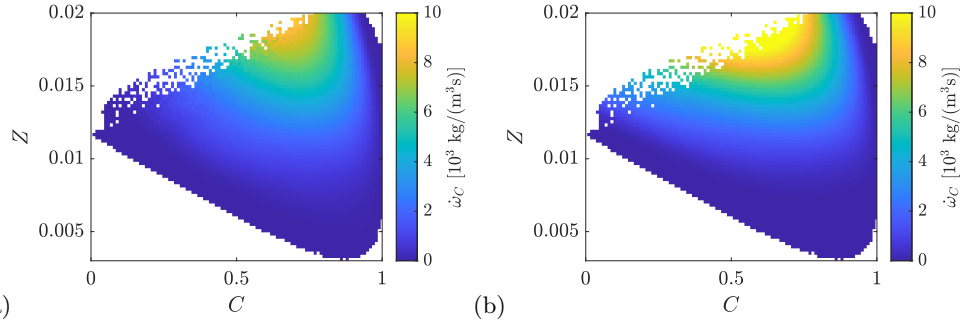

FIGURE 4. (a) Conditionally averaged progress variable source term with respect to mixture fraction and progress variable and (b) model prediction of progress variable source by the set of unstretched premixed flamelets.

with different equivalence ratios. It is evident that the strained flamelets can only parameterize a small portion of the entire flame state, while the set of unstretched flamelets can cover almost the entire joint distribution. Thus, the set of unstretched flamelets is used for modeling, as already proposed by Bastiaans *et al.* (2007) and Regele *et al.* (2013). In the following, it is assessed whether these representative flamelets can accurately describe the progress variable source term in a turbulent flow.

Since the set of unstretched flamelets does not feature any overlaps, building a table to predict $\dot{\omega}_C(C, Z)$ is straightforward. A comparison of the table prediction $\dot{\omega}_C^{\mathrm{FL}}$ and the conditional average $\langle \dot{\omega}_C | C, Z \rangle$ of the DNS data is shown in Figure 4. While certain differences are seen in regions with high mixture fractions, which are characterized by high values of curvature, good qualitative agreement is observed overall and, in particular, at flame states of high probability, cf. Figure 3. As will be shown quantitatively below, low modeling errors are achieved with this model.

Finally, for LES, a model for the subfilter distribution $\mathcal{P}(C, Z)$ is required. The joint distribution $\mathcal{P}(C, Z)$ is shown in Figure 3 and it is evident that progress variable and mixture fraction are not independent of each other. This effect is also reflected by the strongly curved trajectories of the unstretched flamelets in Figure 3(b), which feature a local minimum for intermediate progress variable values. To transform mixture fraction and progress variable into a set of independent variables, which significantly simplifies the modeling of $\mathcal{P}(C, Z)$, the joint distribution of progress variable and a flamelet index is investigated. The latter is the value of the global equivalence ratio ϕ^{FL} for each un-

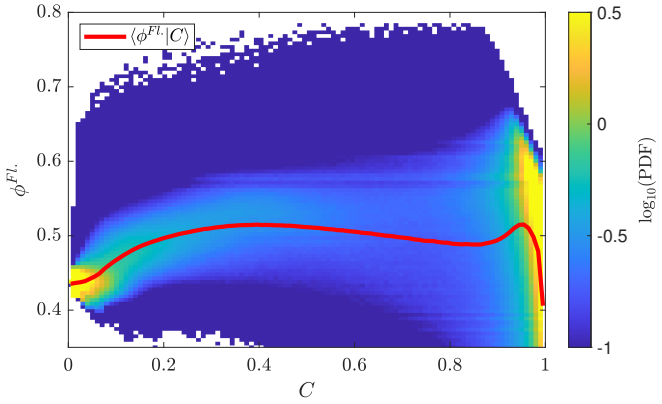

FIGURE 5. Joint distribution of progress variable and the flamelet index of the set of unstretched premixed flamelets with different equivalence ratios.

stretched flamelet in Figure 3(b) and, hence, is constant within a flamelet. Thus, ϕ^{FL} accounts for the transition toward leaner or richer flamelets due to differential diffusion and is independent of progress variable, while mixture fraction also changes within one individual flamelet and, hence, is not independent of progress variable. Using the flamelet table based on the set of unstretched premixed flamelets, ϕ^{FL} is computed for each DNS data point and the joint distribution $\mathcal{P}(C, \phi^{\mathrm{FL}})$ is shown in Figure 5. As expected, ϕ^{FL} and C are statistically almost independent. Also note that on average, combustion occurs on a richer flamelet of $\phi^{\mathrm{FL}} \approx 0.5$ compared to the nominal value of $\phi^{\mathrm{FL}} = 0.4$, which is consistent with the analysis of Berger *et al.* (2022*b*), who showed that combustion occurs at richer mixtures due to the mean positive strain rate in the turbulent flame.

As ϕ^{FL} and C may be assumed to be statistically independent and similar to the model of Knudsen *et al.* (2013) for strongly strained methane/air flames, the following presumed PDF is proposed

$$\mathcal{P}(C, \phi^{\mathrm{FL}}) = \beta(C; \widetilde{C}, \widetilde{C''^2})\delta(\phi^{\mathrm{FL}} - \hat{\phi}^{\mathrm{FL}}). \tag{3.7}$$

A β-PDF is assumed for C, whose shape parameters are determined by $\widetilde{C}$ and $\widetilde{C''^2}$, and a δ-PDF is assumed for the flamelet index ϕ^{FL}. The parameter $\hat{\phi}^{\mathrm{FL}}$ is implicitly given by $\hat{\phi}^{\mathrm{FL}}(\widetilde{C}, \widetilde{Z}, \widetilde{C''^2})$, as will be shown in the following. Further, the assumption of a β-PDF for C is possible, as C is strictly bound to $C \in [0, 1]$. With Eq. (3.7), the filtered source term can be expressed as

$$\overline{\dot{\omega}}_C = \int \dot{\omega}_C(C, \phi^{\mathrm{FL}}) \cdot \beta(C; \widetilde{C}, \widetilde{C''^2})\delta(\phi^{\mathrm{FL}} - \hat{\phi}^{\mathrm{FL}})\, \mathrm{d}C\mathrm{d}\phi^{\mathrm{FL}}, \tag{3.8}$$

$$= \int \dot{\omega}_C(C, \hat{\phi}^{\mathrm{FL}}) \cdot \beta(C; \widetilde{C}, \widetilde{C''^2})\, \mathrm{d}C. \tag{3.9}$$

In particular, the expression in Eq. (3.9) corresponds to the integral of the source term and the β-PDF for a particular flamelet with global equivalence ratio $\hat{\phi}^{\mathrm{FL}}$. To find the correct value of $\hat{\phi}^{\mathrm{FL}}$, the analogous expression for the determination of $\widetilde{Z}$ is exploited

$$\widetilde{Z} = \int Z(C, \phi^{\mathrm{FL}}) \cdot \beta(C; \widetilde{C}, \widetilde{C''^2})\delta(\phi^{\mathrm{FL}} - \hat{\phi}^{\mathrm{FL}})\, \mathrm{d}C\mathrm{d}\phi^{\mathrm{FL}}, \tag{3.10}$$

$$= \int Z(C, \hat{\phi}^{\mathrm{FL}}) \cdot \beta(C; \widetilde{C}, \widetilde{C''^2})\, \mathrm{d}C. \tag{3.11}$$

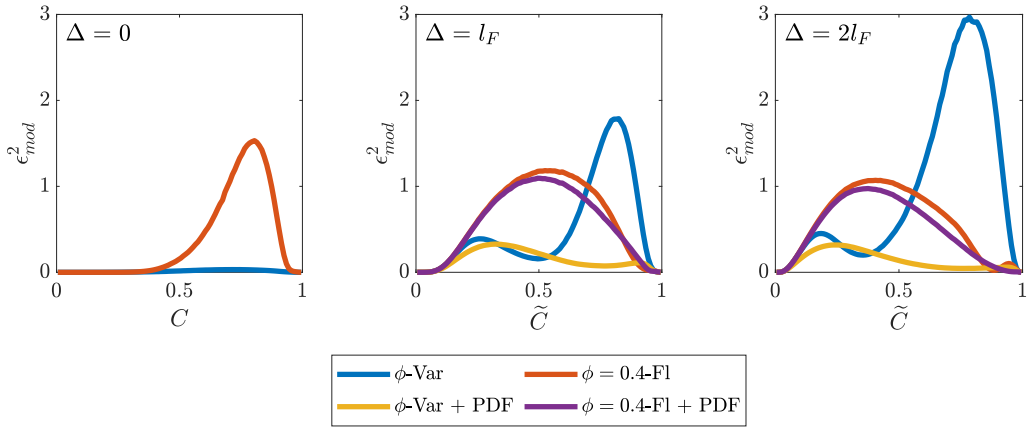

FIGURE 6. Modeling errors of the progress variable source term for three different filter sizes $\Delta = 0$, $\Delta = l_\mathrm{F}$ and $\Delta = 2l_\mathrm{F}$ for four different flamelet-based models.

After computing the integral in Eq. (3.11) for all different flamelets, the value $\hat{\phi}^\mathrm{FL}$ is given by the flamelet that matches the value of the filtered progress variable $\widetilde{Z}$.

In practice, a table can be built directly as a function of $\widetilde{C}$, $\widetilde{Z}$ and $\widetilde{C''^2}$. For this, Eqs. (3.9) and Eq. (3.11) are computed for each flamelet for a prespecified grid of $\widetilde{C}$ and $\widetilde{C''^2}$ values, which is given by the table resolution. Since $\widetilde{Z}$ monotonically increases with $\hat{\phi}^\mathrm{FL}$, the data can be interpolated from the $(\widetilde{C}, \widetilde{C''^2}, \hat{\phi}^\mathrm{FL})$-space to the $(\widetilde{C}, \widetilde{C''^2}, \widetilde{Z})$-space.

3.4. A-priori *model assessment*

Figure 6 shows the assessment of four different combustion models for three different filter sizes. The following models are considered for the comparison:

1) model $\phi = 0.4$-*Fl.* uses a single flamelet at the nominal equivalence ratio, neglecting the effects of a subfilter distribution;

2) model $\phi = 0.4$-*Fl.+PDF* uses a single flamelet at the nominal equivalence ratio and additionally considers the effects of a subfilter distribution by a presumed β-distribution for progress variable. This is a common model for turbulent premixed flames of conventional fuels when thermodiffusive instabilities are not present (Pfitzner 2021);

3) model ϕ-*Var.* describes the local mixture fraction fluctuations by a series of unstretched premixed flamelets with varying equivalence ratio according to Bastiaans *et al.* (2007) and Regele *et al.* (2013). However, the effects of the subfilter distribution are neglected; and

4) model ϕ-*Var.+PDF* is the model described in the previous section and additionally considers the presumed PDF of Eq. (3.7) to account for the complex subfilter fluctuations of mixture fraction and progress variable.

Figure 6 shows the conditionally averaged modeling error as a function of progress variable. The modeling error is defined as

$$\epsilon^2_\mathrm{mod.} = \frac{(\dot{\omega}_C - \dot{\omega}_C^\mathrm{mod})^2}{\max[\langle \dot{\omega}_C | C \rangle^2]}, \tag{3.12}$$

where the same normalization as for the irreducible errors is chosen. This definition compares the absolute modeling errors with the maximum average progress variable source term within the flame. Note that the value of the normalization is constant for

one particular filter size but decreases for increasing filter size, as filtering reduces the maximum value of the progress variable source term.

For the unfiltered DNS data, a significant reduction of modeling errors is observed by the multiple flamelet model ϕ-*Var.* with respect to the single flamelet model $\phi = 0.4$-*Fl.*, which neglects the effects of differential diffusion. In particular, the modeling errors for the ϕ-*Var.* model are almost zero, indicating an accurate representation of the flame state by the series of unstretched premixed flamelets. For the filtered fields, the single flamelet model $\phi = 0.4$-*Fl.* again shows high modeling errors, which does not significantly change for the $\phi = 0.4$-*Fl.+PDF* model that additionally considers a subfilter distribution. These two models entirely neglect the effects of local mixture fraction fluctuations, so their failure is expected. It is worth noting that a value of unity indicates a significant error, as the modeling errors are as large as the maximum value of the conditionally averaged progress variable source term. Further, the modeling errors of model ϕ-*Var.* are seen to increase with increasing filter size. This results from a strong overprediction of the progress variable source term by the model, as it does not consider the effect of filtering. In particular, filtering leads to a reduction of the peak reaction rates. In contrast, the newly proposed model ϕ-*Var.+PDF*, which accounts for the effects of a subfilter distribution by means of the presumed PDF in Eq. (3.7), yields a significant reduction of modeling errors.

4. Conclusions

In this work, an LES combustion model for turbulent hydrogen flames has been developed and validated by means of DNS data. In particular, the new combustion model can account for the effects of thermodiffusive instabilities, which have a leading order effect in hydrogen flames. In an optimal estimator analysis, mixture fraction, progress variable and the variance of progress variable are identified as suitable parameters to adequately parameterize the fluctuations of the progress variable source term that are caused by thermodiffusive instabilities. Similar to previous work of Bastiaans *et al.* (2007) and Regele *et al.* (2013), the model is built on a set of unstretched premixed flamelets with different equivalence ratios, which is shown to accurately describe the instantaneous progress variable source term. To model the flame/turbulence subfilter interactions, a presumed PDF based on a flamelet index and progress variable is proposed. The subfilter PDF is modeled by a β-distribution for the progress variable and a δ-distribution for the flamelet index. The latter assumes that combustion occurs within a subfilter volume along one particular flamelet, the equivalence ratio of which is chosen dynamically. An *a-priori* analysis of the newly suggested combustion model indicates a significant reduction of modeling error in comparison to models that do not account for thermodiffusive instabilities. Particularly, the introduction of the new subfilter PDF model is shown to be of high relevance for the filtered fields. An *a-posteriori* analysis of the newly proposed model is planned for the future.

Acknowledgments

The authors thank Thierry Poinsot, Andrea Aniello and Davide Laera for fruitful discussions during the CTR Summer Program.

REFERENCES

Ahmed, P., Thorne, B., Lawes, M., Hochgreb, S., Nivarti, G. V. & Cant, R. S. 2021 Three dimensional measurements of surface areas and burning velocities of turbulent spherical flames. *Combust. Flame* **233**, 111586.

Aspden, A. J., Day, M. S. & Bell, J. B. 2011 Turbulence-flame interactions in lean premixed hydrogen: transition to the distributed burning regime. *J. Fluid Mech.* **680**, 287–320.

Bastiaans, R., Vreman, A. & Pitsch, H. 2007 DNS of lean hydrogen combustion with flamelet-generated manifolds. *Annual Research Briefs,* Center for Turbulence Research, Stanford University pp. 195–206.

Berger, L., Attili, A. & Pitsch, H. 2022*a* Intrinsic instabilities in premixed hydrogen flames: parametric variation of pressure, equivalence ratio, and temperature. part 2 – Non-linear regime and flame speed enhancement. *Combust. Flame* **240**, 111936.

Berger, L., Attili, A. & Pitsch, H. 2022*b* Synergistic interactions of thermodiffusive instabilities and turbulence in lean hydrogen flames. *Combust. Flame* **244**, 112254.

Berger, L., Kleinheinz, K., Attili, A. & Pitsch, H. 2019 Characteristic patterns of thermodiffusively unstable premixed lean hydrogen flames. *Proc. Combust. Inst.* **37**, 1879–1886.

Bilger, R. W., Starner, S.H. & Kee, R. J. 1990 On reduced mechanisms for methane-air combustion in nonpremixed flames. *Combust. Flame* **80**, 135–149.

Giannakopoulos, G. K., Gatzoulis, A., Frouzakis, C. E., Matalon, M. & Tomboulides, A. G. 2015 Consistent definitions of "Flame Displacement Speed" and "Markstein Length" of premixed flame propagation. *Combust. Flame* **162**, 1249–1264.

Knudsen, E., Kolla, H., Hawkes, E. R. & Pitsch, H. 2013 LES of a premixed jet flame DNS using a strained flamelet model. *Combust. Flame* **160**, 2911–2927.

Luca, S., Attili, A., Schiavo, E. L., Creta, F. & Bisetti, F. 2019 On the statistics of flame stretch in turbulent premixed jet flames in the thin reaction zone regime at varying Reynolds number. *Proc. Combust. Inst.* **37**, 2451–2459.

Matalon, M. 2007 Intrinsic flame instabilities in premixed and nonpremixed combustion. *Annu. Rev. Fluid Mech.* **39**, 163–191.

Perner, J. & Bothe, D. 2018 Report for the World Energy Council German by Frontier Economics Ltd.

Pfitzner, M. 2021 A new analytic pdf for simulations of premixed turbulent combustion. *Flow Turbul. Combust.* **106**, 1213–1239.

Pitsch, H. 1998 A C++ program package for 0-d combustion and 1-d laminar flames., *Aachen, unpublished*

Regele, J. D., Knudsen, E., Pitsch, H. & Blanquart, G. 2013 A two-equation model for non-unity Lewis number differential diffusion in lean premixed laminar flames. *Combust. Flame* **160**, 240–250.

Sartbaeva, A., Kuznetsov, V. L., Wells, S. A. & Edwards, P. P. 2008 Hydrogen nexus in a sustainable energy future. *Energ. Environ. Sci.* **1**, 79–85.

Schlup, J. & Blanquart, G. 2019 Reproducing curvature effects due to differential diffusion in tabulated chemistry for premixed flames. *Proc. Combust. Inst.* **37**, 2511–2518.